



Enhanced selective adsorption of H₂S from CO₂ by incorporating methylated polyethyleneimine into a porous carbon matrix

Lan Luo, Chunliang Yang, Fei Liu*, Quanlan Liao, Peng Chen, Tianxiang Zhao*

Key Laboratory of Green Chemical and Clean Energy Technology, School of Chemistry and Chemical Engineering, Guizhou University, Guiyang 550025, PR China



ARTICLE INFO

Keywords:
CO₂ adsorption
H₂S
Selective separation
Amine-functionalized
Porous carbon

ABSTRACT

In this study, a series of hybrid adsorbent materials (AC@mPEI) with superior selective separation properties of H₂S and CO₂ are prepared by taking advantage of the differences in reaction mechanisms between H₂S and CO₂, as well as tertiary amines. Using a straightforward impregnation method, the methylated polyethyleneimine (mPEI) is successfully introduced into the pores of the porous carbon to create the desired hybrid adsorbents. The strong interaction between the tertiary amine groups and H₂S facilitates the selective separation of H₂S and CO₂ gases. Remarkably, the adsorbent (1:1)AC@mPEI exhibits a substantial H₂S adsorption capacity of 5.83 mmol·g⁻¹ at 298 K and 1.0 bar and a high separation selectivity of H₂S to CO₂ (133), which is approximately 16.6 times higher than that of the porous carbon supporter. Further investigations, involving adsorption thermodynamics, breakthrough experiments, and spectroscopy, confirm that the strong interaction between the hybrid materials and H₂S plays a pivotal role in enhancing the separation selectivity of H₂S. Additionally, the adsorbed H₂S can be well desorbed through vacuum degassing, allowing for multiple cycles of the adsorbent. This strategy, which leverages differences in gas adsorption mechanisms to fabricate hybrid adsorbents, presents novel concepts for the development of functional adsorbent materials for selective separation of gases.

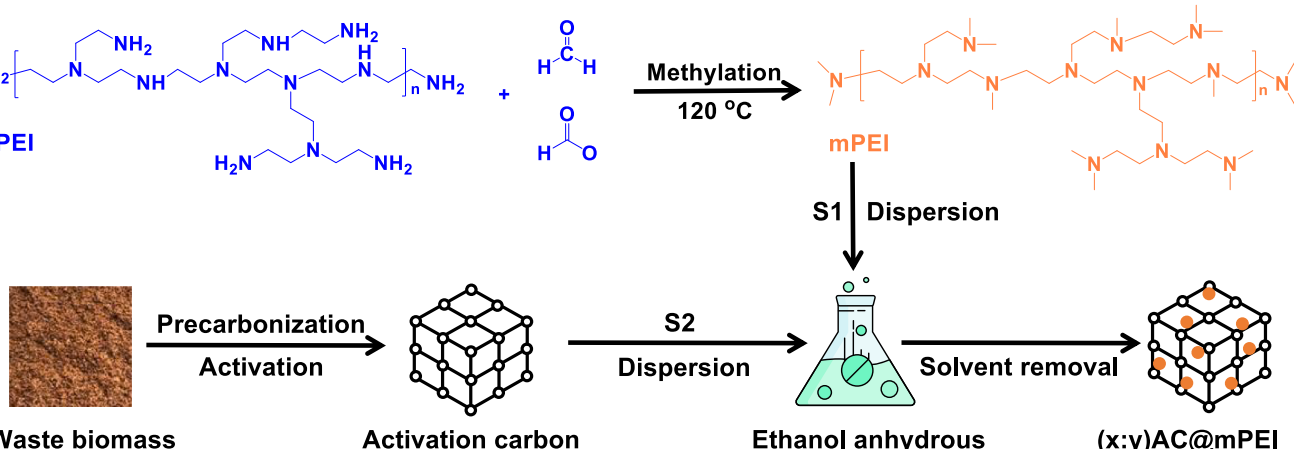
1. Introduction

The increase in energy demand has led to a higher reliance on natural gas, which is a fossil fuel and one of the main sources of energy. However, the use of natural gas has a significant impact on the environment [1]. Natural gas is predominantly composed of hydrocarbons, specifically alkanes, along with trace heavy hydrocarbons and non-hydrocarbon gases such as nitrogen (N₂), carbon dioxide (CO₂), and hydrogen sulfide (H₂S). H₂S is a highly toxic, colorless, and flammable acid gas that gives off a foul odor similar to rotten eggs. During the purification process of natural gas, acid gases, especially H₂S, can be absorbed by water, resulting in severe corrosion of industrial equipment and pipeline facilities [2]. It has been reported that airborne H₂S can be captured by water, leading to the production of acid rain and subsequent acidification of terrestrial aquatic systems [3]. Moreover, the combustion of natural gas also represents a significant contributor to atmospheric CO₂ emissions, posing an imminent threat to Earth's climate [4,5]. Therefore, it is crucial to develop and advance technologies for removing H₂S and CO₂ in order to ensure compliance with environmental and safety regulations across diverse industries.

Considering the coexistence of H₂S and CO₂ in most emission sources [6], two types of separation technologies are generally adopted for their removal: (1) simultaneous removal of H₂S and CO₂, and (2) selective removal of either H₂S or CO₂ [7]. The most common technology for simultaneous removal of H₂S and CO₂ is absorption, which utilizes amines [8,9], alkaline salts [10], and physical solvents [11,12]. However, the absorption process still faces challenges such as volatile corrosion, high viscosity, difficult degradation, and high consumption of renewable energy [13]. Moreover, H₂S and CO₂ exhibit competitive behavior during transportation, and the synchronous removal of both gases reduces the efficiency of H₂S removal, necessitating further refinement of gas treatment. It should be noted that simultaneous removal technology is mainly suited for high concentration gas sources and requires more complex material design and operating parameters. Among the existing separation technologies for selective removal of H₂S or CO₂, the most commonly used methods are absorption [14,15], adsorption [16,17], and membrane separation [18,19]. Researchers have proposed that the use of porous solid adsorbent materials for adsorption is the most-effective and environmentally friendly separation technology [20–22]. This technology not only avoids the volatility,

* Corresponding authors.

E-mail addresses: ce.feiliu@gzu.edu.cn (F. Liu), txzhao3@gzu.edu.cn (T. Zhao).



Scheme 1. Schematic illustration of the synthesized AC@mPEI.

viscosity, and corrosion problems associated with liquid absorbers but also has lower energy consumption compared to membrane separation technology. So far, extensive research has been conducted on various solid adsorbents (such as porous carbon materials [23,24], zeolites [25,26], porous polymers [27,28], and metal-organic frameworks (MOFs) [29,30]) with different structural properties for the removal of low concentration H_2S or CO_2 gas. Particularly, porous carbon materials possess large surface area, high thermal stability, and adjustable chemical structure [31,32], making them reasonable candidates for the removal of H_2S . Unfortunately, conventional porous carbon materials tend to have low selectivity for $\text{H}_2\text{S}/\text{CO}_2$, $\text{H}_2\text{S}/\text{N}_2$, and $\text{H}_2\text{S}/\text{CH}_4$ during the adsorption process [33,34].

To enhance the efficient capture of CO_2 , porous carbon can be loaded with amines that have alkaline adsorption sites and strongly interact with gas molecules. Various amines are loaded into porous carbon to improve the separation of gases. Typically, polyethylenimine (PEI) with low volatility, which contains abundant $-\text{NH}_2$ groups, is the preferred enhancer for loading alkaline groups onto porous carbon [35]. Furthermore, the separation selectivity of the gas can also be regulated by methylating the $-\text{NH}_2$ groups. In 2020, Lan *et al.* [36] prepared mPEI@g-C₃N₄ by physical supporting methylated polyethylenimine (mPEI) on g-C₃N₄ and used to capture SO_2 . The ideal solution adsorption theory (IAST) selectivity of $\text{SO}_2/\text{CO}_2(10/90)$ and $\text{SO}_2/\text{N}_2(10/90)$ reached 630 and 14,607 at 25 °C and 1 bar, respectively. Huang *et al.* [37] synthesized PTA@PDVB composite sorbent by loading tertiary amines onto meso-macroporous polymer for SO_2 capture. The sorbents exhibited SO_2 adsorption capacities ranging from 3.86 to 6.88 mmol·g⁻¹ at 25 °C and 0.002 bar. Recently, Kan *et al.* [38] utilized F-Ce-MOF-SC-x as a stable carrier for anchoring polytertiary amines (PA) via coordination interactions with Ce-DUS. Due to the superior ability of PA to recognize SO_2 , the resulting F-Ce-MOF-SC-x@yPA demonstrated outstanding performance in high-temperature reversible adsorption and separation of SO_2 . This research illustrates that tertiary amine groups have a selective interaction with highly acidic SO_2 molecules, leading to successful separation of SO_2/CO_2 gases. Furthermore, porous solid materials such as above g-C₃N₄, PDVB, and F-Ce-MOF-SC-x can act as stable carriers supporting tertiary amine groups, thereby improving the cyclic stability of hybrid adsorbent materials in gas adsorption and separation applications. Likewise, the stronger interaction between tertiary amine groups and H_2S , which is due to the presence of active hydrogen and greater acidity, offers the potential for selectively separating H_2S in mixed gas streams. However, no relevant reports have been found regarding the utilization of porous adsorbents incorporating tertiary amines for the selective separation of H_2S in previous studies.

In our previous study [39], we successfully developed a distillers' grains-based porous carbon with a remarkable CO_2 adsorption capacity

of 7.02 mmol·g⁻¹ at 273 K and 1 bar. Despite these achievements, the selective separation of CO_2 and H_2S remains a significant challenge, as the IAST selectivity for $\text{H}_2\text{S}/\text{CO}_2$ (2/98) is only 8. The current work is dedicated to improving separation selectivity of low concentration H_2S and CO_2 , a series of hybrid adsorbent materials (AC@mPEI) thus fabricated by using mPEI interspersed in the distillers' grains-based porous carbon. The aim of this work is to utilize the abundant heteroatoms (O, N, H), high porosity, high specific surface area, and high thermal stability of porous carbon. This involves using activated carbon (AC) as solid support to disperse mPEI within the porous carbon skeleton in order to enhance exposure and increase the contact between tertiary amine groups and gas molecules. The goal is to improve the selective separation of $\text{H}_2\text{S}/\text{CO}_2$ by leveraging the differences in electronic interactions between polar H_2S and linear CO_2 , and tertiary amine groups. Additionally, the design of the hybrid adsorbent aims to retain a portion of the porosity and specific surface area while facilitating the diffusion, mass transfer, and concentration of gas molecules through the pores to enhance the adsorption performance of the hybrid adsorbent. Furthermore, the high thermal stability of porous carbon as a solid support can effectively prevent the decomposition and loss of mPEI during the gas adsorption reaction. The superior separation selectivity of H_2S and CO_2 was acquired by taking advantage of the differences in reaction mechanisms between H_2S and CO_2 , as well as the presence of tertiary amines. Compared with porous carbon alone, the separation selectivity was increased by 16.6 times for the optimized adsorbent (1:1)AC@mPEI. The detailed mechanism insight reveals that the strong interaction between the hybrid materials and H_2S is crucial for enhancing the separation selectivity of H_2S .

2. Materials and methods

2.1. Chemicals

Polyethylenimine (PEI, M_n:600), thiourea (>99.5 %), KOH (>90 %), HCl (36 %), formic acid (>99 %), formaldehyde (38 % in water), and chloroform-d (CDCl_3 , 99.96 %) were purchased from Adamas Beta (Shanghai) Chemical Reagent Co., Ltd. China. H_2S (99.9 %), CO_2 (99.99 %), N_2 (99.999 %), and CH_4 (99.99 %) were purchased from Guiyang Sanhe Gas Center, Guizhou, China.

2.2. Characterization

¹H NMR and ¹³C NMR spectra were measured on a JNM-ECZ-400 spectrometer at 400 MHz and 101 MHz, respectively. N_2 adsorption-desorption isotherms were measured on a micrometrics ASAP 2460 instrument at a temperature of -196 °C to investigate the pores

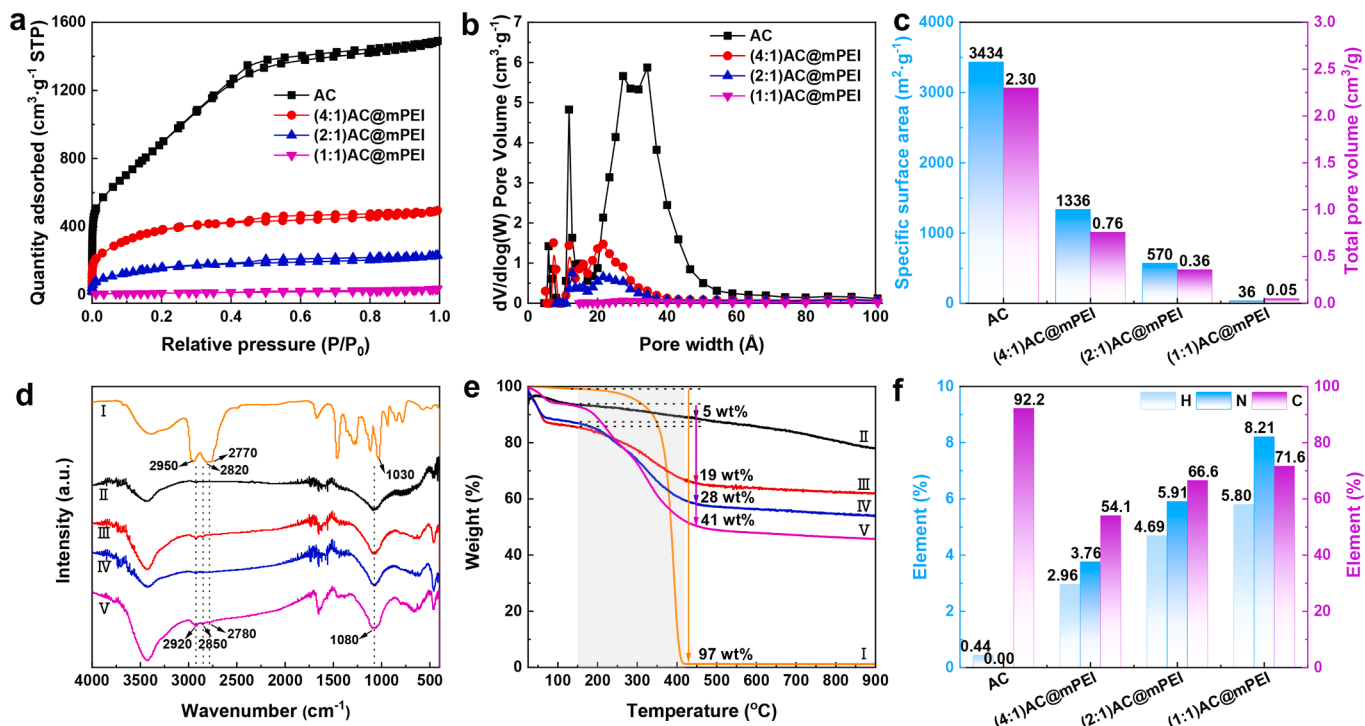


Fig. 1. N₂ adsorption–desorption isotherms (a), average pores size distributions (b), and pores structural features (c) of AC and (x:y)AC@mPEI; FTIR spectra (d) and TGA curves (e) of AC and (x:y)AC@mPEI; (I) mPEI, (II) AC, (III) (4:1)AC@mPEI, (IV) (2:1)AC@mPEI, (V) (1:1)AC@mPEI; surface compositions of the adsorbents measured by element analysis (f).

structure properties of adsorbents. FTIR spectra were collected on a Nicolet iS50 FTIR spectrometer. Thermogravimetric analysis (TGA) was conducted on a NETZSCH STA449F5 instrument to obtain the TGA curves. The morphology and microstructure of as-prepared adsorbents were observed using a Nitachi S-3400 N scanning electron microscope (SEM) and a PEI G2 F20 transmission electron microscope (TEM). The elemental composition and valence state of the elements in the adsorbents were measured using a UNICUBE elementar instrument and a Thermo Fisher K-Alpha plus X-ray electron spectroscopy (XPS) instrument.

2.3. Synthesis of (x:y)AC@mPEI

The distillers' grains-based porous carbon (AC) was prepared following our previous work [39]. mPEI was synthesized in accordance with the method reported in the literature [40,41], and the ¹H NMR spectrum of mPEI is shown in Fig. S1. The (x:y)AC@mPEI hybrid materials were prepared by impregnating mPEI into the pre-prepared AC, as shown in Scheme 1 and Fig. S2 for photographs. Typically, AC ($x = 200$ mg) and mPEI ($y = 50, 100, 200, 300$ mg) were mixed in 20 mL of ethanol, followed by ultrasound for 1 h and stirring at room temperature for 24 h, and finally the ethanol was removed and freeze-dried overnight to obtain a hybrid adsorbent (x:y)AC@mPEI, where x:y is the mass ratio of AC to mPEI. As a control experiment, (1:1)AC@PEI was prepared by replacing mPEI with PEI.

2.4. Gas adsorption

The adsorption capacity of H₂S was assessed using a static equilibrium adsorption method involving a double kettle, as described in our previous work [42]. The non-corrosive gases such as CO₂, N₂, and CH₄ were tested using a micrometrics BSD-PM2 instrument. All experiments were conducted at temperatures ranging from 298 to 333 K and pressures ranging from 0 to 1.5 bar, using about 100 mg of adsorbent. The selectivity of the adsorbents for H₂S relative to CO₂ (2/98), N₂ (1/99),

and CH₄ (10/90) at 298 K was evaluated using the IAST equation. The breakthrough experiments for the mixed gas were tested at 298 K using a BSD-MAB multi-constituent adsorption breakthrough curve analyzer. Before the test, about 0.2 g of adsorbent was activated at 150 °C for 5 h. The flow rate of the mixed gas was maintained at 10 mL·min⁻¹, and the concentration of the outflow gas was detected monitored online with a mass spectrometer.

3. Results and discussion

3.1. Characterization of adsorbents

The textural parameters of AC and hybrid adsorbent materials (x:y)AC@mPEI were characterized using N₂ adsorption–desorption isotherms and average pores size distributions, respectively. Fig. 1a shows that the N₂ adsorption isotherm of AC displays both type I and IV shapes according to the International Union of Pure and Applied Chemistry (IUPAC) classification. There is a significant N₂ adsorption amount at low relative pressure ($p/p_0 < 0.1$) and a hysteresis loop at moderate relative pressure ($0.4 < p/p_0 < 0.8$), implying the well-developed microporous and mesoporous structures of AC. This observation is further supported by the pores size distributions (Fig. 1b). After interspersing of mPEI onto AC, (4:1)AC@mPEI shows a similar N₂ adsorption–desorption isotherm shape to AC, but the N₂ adsorption amount significantly decreases, and the pores size distributions narrow down to the range of 0–4 nm. As the loading of mPEI increases, the N₂ uptake of the hybrid adsorbent materials gradually decreases and the hysteresis loop even disappears for (1:1)AC@mPEI. The pores size distributions also gradually decrease in the following order: (1:1)AC@mPEI < (2:1)AC@mPEI < (4:1)AC@mPEI < AC. The specific surface area (S_{BET}) and total pore volume (V_t) of these adsorbents were also calculated, as shown in Fig. 1c. It is found that AC has the highest S_{BET} of 3434 m²·g⁻¹ and the highest V_t of 2.30 cm³·g⁻¹ due to the presence of abundant microporous and mesoporous structures. As the loading of mPEI increases, the S_{BET} and V_t of hybrid adsorbent materials gradually

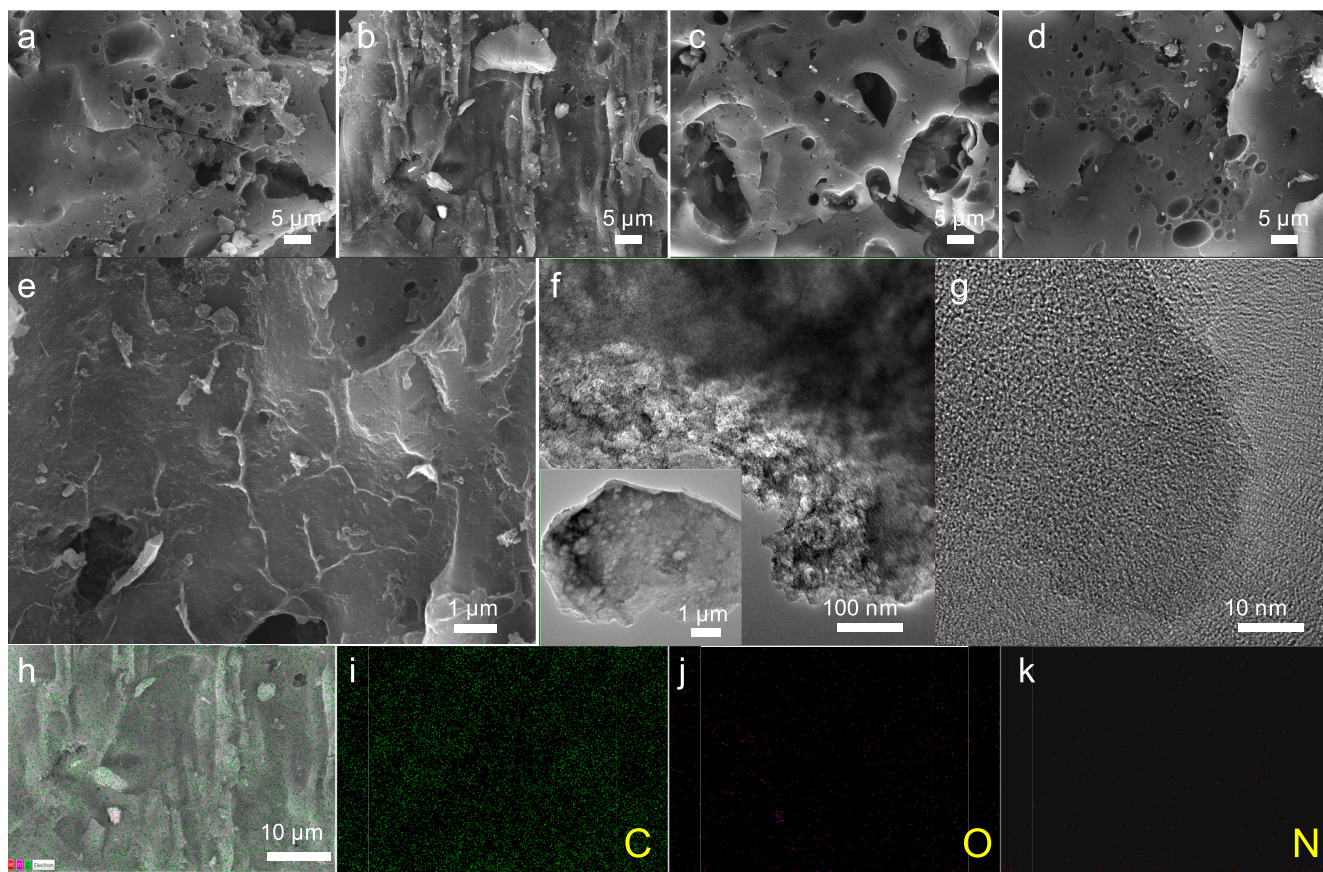


Fig. 2. SEM of AC (a), (1:1)AC@mPEI (b), (2:1)AC@mPEI (c), and (4:1)AC@mPEI (d); enlarged Fig. 2b (e), TEM (f, g), SEM of (1:1)AC@mPEI (h), and elemental mapping images (i-k) of (1:1)AC@mPEI.

decrease, which can be attributed to the pores of AC being gradually occupied by loaded mPEI. Observably, the drop dramatically S_{BET} of 36 $\text{m}^2 \cdot \text{g}^{-1}$ and V_t of 0.05 $\text{cm}^3 \cdot \text{g}^{-1}$ of (1:1)AC@mPEI indicate dispersion and fixation of mPEI in carbon skeleton.

The FTIR spectra of Fig. 1d exhibit the absorption peaks at 2950, 2820, and 2770 cm^{-1} , which correspond to the stretching vibration of $-\text{CH}_2-$ groups of mPEI. The band observed at 1030 cm^{-1} is attributed to the stretching vibration of C-N bond [38]. All characteristic peaks of mPEI are appearing in the FTIR spectra of (x:y)AC@mPEI. As the loading of mPEI increases, the intensity of these bands also increases, with the characteristic peaks of mPEI becoming particularly prominent in the FTIR spectra of (1:1)AC@mPEI. Moreover, no new bonds or significant shifts in characteristic peaks were observed in the FTIR spectra of any of hybrid adsorbent materials. These results suggest that loading of mPEI into AC occurs through physical interactions.

The thermal stability of (x:y)AC@mPEI, mPEI, and PEI was tested, respectively. There are two major weight loss in the TGA curve of PEI, as shown in Fig. S3 spanning 50–200 °C and 300–375 °C. This weight can be attributed the evaporation of volatile impurities and the decomposition of PEI, respectively. In contrast, mPEI only has one major weight loss at temperatures of 300–420 °C, corresponding to the decomposition temperature of mPEI. It is evident that mPEI exhibits slightly higher stability than PEI, potentially attributed to the decomposition temperature of $-\text{CH}_3$ groups being higher than that of $-\text{NH}_2$ [43]. Fig. 1e shows that AC exhibits a weight loss of 22 % over the entire temperature range from 25 to 900 °C, which is significantly lower than that of mPEI. This indicates excellent thermal stability of AC. For (x:y)AC@mPEI, all TGA curves exhibit three weight loss regions. The first region is attributed to volatile impurities evaporation, the second region corresponds to mPEI decomposition, and the third region is attributed to AC decomposition. In the temperature range of 150 to 420 °C, as the mPEI loading

increases, the weight loss follows this order: AC (5 %) < (4:1)AC@mPEI (19 %) < (2:1)AC@mPEI (28 %) < (1:1)AC@mPEI (41 %) < mPEI (97 %). The thermal stability of (1:1)AC@mPEI is significantly higher than that of mPEI when the loading of mPEI reaches an equal mass to AC. This can be attributed to the pore restriction effect of AC, which delays the weight loss of loaded mPEI. Elemental analysis, as shown in Fig. 1f, demonstrated the elemental compositions of AC and (x:y)AC@mPEI. No N was detected in AC, whereas the N content of hybrid adsorbent materials increased to 3.76–8.21 % with increasing mPEI loading. The results confirmed the successful preparation of (x:y)AC@mPEI and demonstrated that AC has high loading capacity for mPEI. Raman spectroscopy was used to characterize the defect structure of AC and (1:1)AC@mPEI, and the results are shown in Fig. S4. After the introduction of mPEI, the peak intensity ratio (I_D/I_G) of D and G of (1:1)AC@mPEI did not change significantly, indicating that the crystal defect of C in the hybrid material remained unchanged. The results show that the introduction of mPEI into porous carbon is mainly achieved through physical loading.

The morphology of AC and (x:y)AC@mPEI was characterized by SEM. Fig. 2a shows that AC exhibits abundant and compact irregular pores. Notably, Fig. 2b-d reveal the increase in mPEI loading in the adsorbents, which leads to a significant morphological change in (x:y)AC@mPEI. One noteworthy observation is the reduction in pores observed in the surface morphology of the adsorbent. Among these adsorbents, the surface of (1:1)AC@mPEI becomes rough with limited pores. This could be attributed to the mPEI occupying a considerable number of pore channels, indicating a uniform distribution of mPEI onto AC and thereby improving the interaction between tertiary amine groups and gas molecules. SEM analysis at a higher magnification reveals that (1:1)AC@mPEI displays folds, suggesting that mPEI is loaded on the surface of the AC (Fig. 2e). To further elucidate the structure of

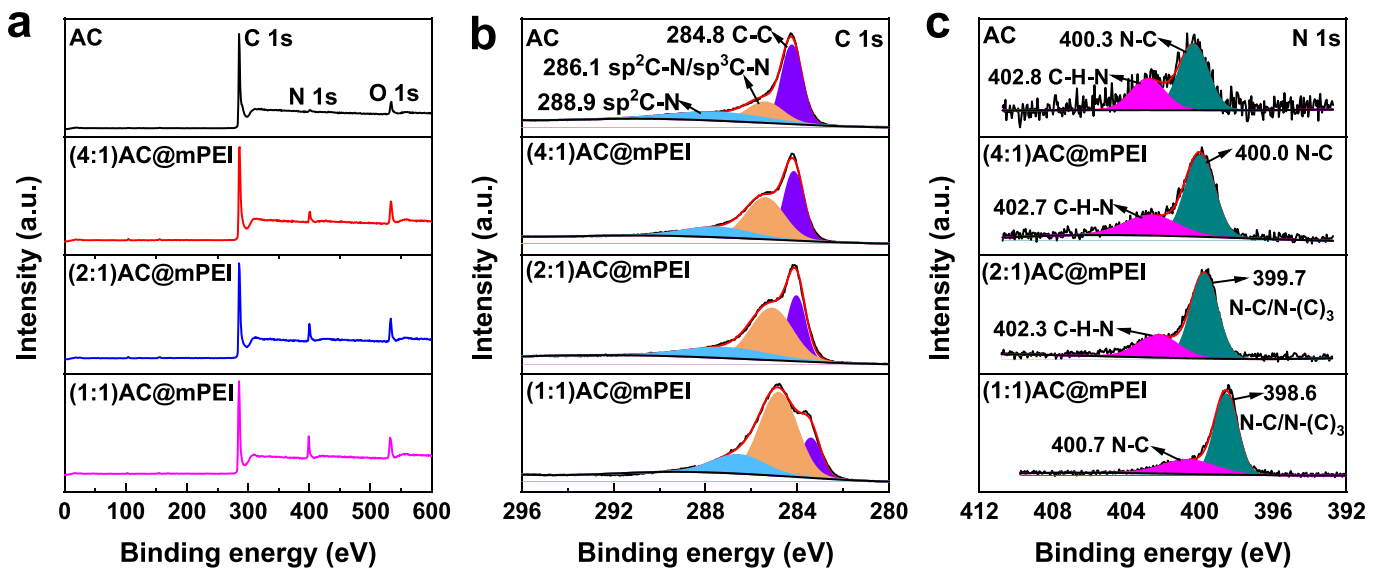


Fig. 3. XPS spectra of the AC and (x:y)AC@mPEI adsorbents: survey spectrum (a), C 1 s spectra (b), and N 1 s spectra (c).

(1:1)AC@mPEI, TEM and elemental mapping were presented in Fig. 2f and g, respectively. As expected from the SEM image, TEM images of (1:1)AC@mPEI display the occupation of pores and a rough surface owing to the presence of mPEI. High-resolution TEM shows that the (1:1)AC@mPEI is amorphous but exhibits typical microporous characteristics (Fig. 2g). Additionally, Fig. 2h-k reveal the random dispersion of C, O, and N elements within the nanostructure of the adsorbent. The presence of N-containing functional groups in the adsorbent facilitates its ability to capture gas molecules.

To investigate the bonding configuration and properties of different groups on the surface of AC and (x:y)AC@mPEI, XPS analysis was performed. Fig. 3a reveals the survey spectra, which includes C 1s, N 1s, and O 1s spectra. However, the intensity of the N 1s in the survey spectrum of AC is weak. Consistent with the survey spectrum, the atomic percentage of N 1s in AC has the smallest value of 1.65 %. Notably, the N 1s atomic percentage increased with increasing mPEI loading in the hybrid adsorbent materials. Among the, (1:1)AC@mPEI exhibits the highest N 1s content of 10.39 %.

The split-peak fitting was carried out to gain insight into the properties of C, N, and O elements in the adsorbents. The C 1s spectra of the four adsorbents display three distinct peaks at around 288.9, 286.1, and 284.8 eV (Fig. 3b). In the case of AC, the peak with the highest binding energy, 288.9 eV, corresponded to sp²-hybridized C atoms in the aromatic rings connected to N-containing groups (C-N). The peak at 286.1 eV is assigned to the sp² C bonded to N inside aromatic rings (C-N), while the lowest binding energy, 284.8 eV, is attributed to the pure graphitic

site in amorphous carbon (C-C) [34]. Notably, with the increase in mPEI loading, the peak area corresponding to the binding energy at 286.1 eV gradually increased due to the presence of the C-N bonding between sp³-hybridized C atoms in -CH₃ and N [44,45]. The N 1s spectra of the four adsorbents exhibit two visible peaks at around 402.3 and 400.3 eV (Fig. 3c). The peak with the higher binding energy, 402.3 eV, is attributed to terminal amino functions [46], while the peak with the lower binding energy, 400.3 eV, is assigned to the N atom strongly bonded to sp² C (N-C) [47]. However, with the addition of mPEI, the peaks shift towards lower binding energy, possibly due to the introduction of N-C bonds and terminal N-CH₃ groups from mPEI. In addition, the O 1s spectra of the four adsorbents display two peaks at around 533.1 eV and 537.1 eV (Fig. S5). These peaks are assigned to C=O (carboxyl groups and carbonyl groups) and C-O (hydroxide radical), respectively. The oxygen atoms are mainly derived from the porous carbon. Therefore, the degree of O1s spectral variation in different adsorbents is small, likely due to the content of porous carbon in hybrid adsorbents, as well as potential influence from the presence of solvent ethanol during synthesis and exposure to air during XPS testing.

3.2. Gas adsorption

3.2.1. Screening of amines

To evaluate the potential organic amines for selective separation of H₂S, we measured the solubility of H₂S and CO₂ in two types amines, PEI and mPEI, at a temperature of 298 K. The experimental results, depicted

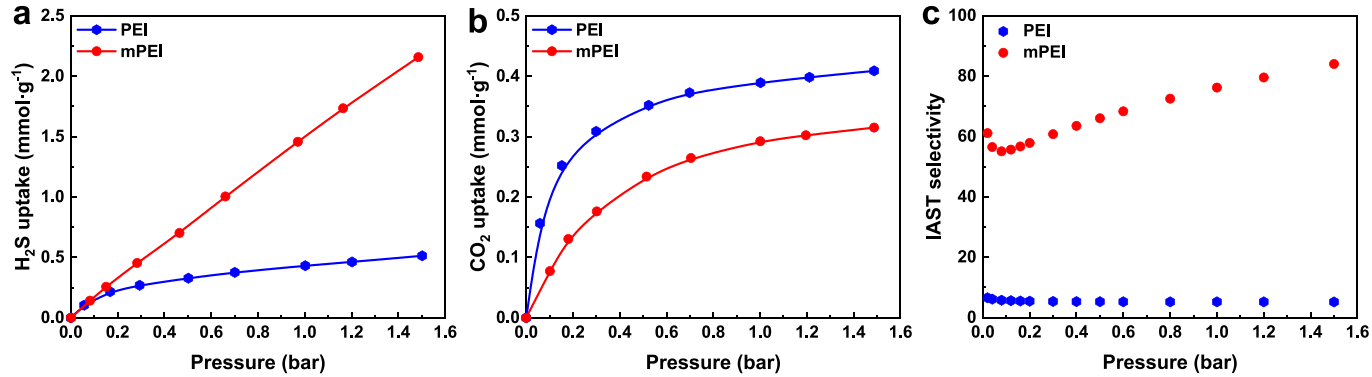


Fig. 4. H₂S adsorption isotherms (a), CO₂ adsorption isotherms (b), and IAST selectivity of H₂S/CO₂(2/98) (c) at 298 K of PEI and mPEI.

Table 1

Gas uptake performance and IAST selectivity at 298 K and 1.0 bar.

Separating medium	Adsorption capacity (mmol·g ⁻¹)				IAST selectivity at 298 and 1.0 bar		
	H ₂ S	CO ₂	N ₂	CH ₄	H ₂ S/CO ₂ (2/98)	H ₂ S/N ₂ (1/99)	H ₂ S/CH ₄ (10/90)
PEI	0.43	0.39	—	—	5	—	—
mPEI	1.46	0.29	—	—	76	—	—
AC	7.07	2.15	0.44	1.10	8	48	18
(4:1)AC@mPEI	5.14	1.14	0.21	0.51	16	170	59
(2:1)AC@mPEI	4.25	0.84	0.17	0.39	29	307	133
(1:1)AC@mPEI	5.83	0.42	0.08	0.16	133	1344	846
(1:1.5)	3.76	0.22	0.05	0.05	40	129	422
AC@mPEI	—	—	—	—	—	—	—
(1:1)AC@PEI	3.04	0.84	0.08	0.18	19	452	451

in Fig. 4a and b, indicate that the tertiary amine groups in mPEI are beneficial for capturing H₂S and inhibiting the adsorption of CO₂. Specifically, the H₂S uptake of mPEI is measured to be 1.46 mmol·g⁻¹ at 298 K and 1.0 bar, which is 3.40 times higher than that of PEI (as

presented in Table 1). Moreover, the IAST selectivity of H₂S/CO₂(2/98) at 298 K of mPEI is significantly improved, reaching the value of 76 at 1.0 bar, being 15.2 times as the selectivity of PEI (Fig. 4c). Based on these findings, it is concluded that mPEI is the preferred choice for injection into AC for the purpose of selective separation of H₂S.

3.2.2. Gas adsorption capacity

The H₂S, CO₂, N₂, and CH₄ adsorption isotherms of the prepared adsorbents were measured at 298 K and 0–1.5 bar. Fig. 5a shows that the H₂S adsorption curve of AC is linear and positively correlated with pressure, suggesting that the adsorption mechanism of AC on H₂S is mainly physical adsorption. The incorporation of mPEI results in significant changes in the H₂S adsorption curves. With an increase in mPEI loading, the isotherms gradually exhibit positive and non-linear correlation between the H₂S adsorption capacities of (x:y)AC@mPEI and pressures, suggesting a transition from physical to chemical adsorption. From Fig. 5b and c, it can be observed that the amount of H₂S adsorption at 1.0 bar decreased from 7.07 mmol·g⁻¹ for AC to 4.25 mmol·g⁻¹ for (2:1)AC@mPEI (Table 1). This decrease can be attributed to the blockage of AC pores by mPEI, resulting in limited volumes for gas molecule storage. It is noteworthy that (1:1)AC@mPEI, with a high H₂S adsorption capacity of 5.83 mmol·g⁻¹ at 1.0 bar, displays superior

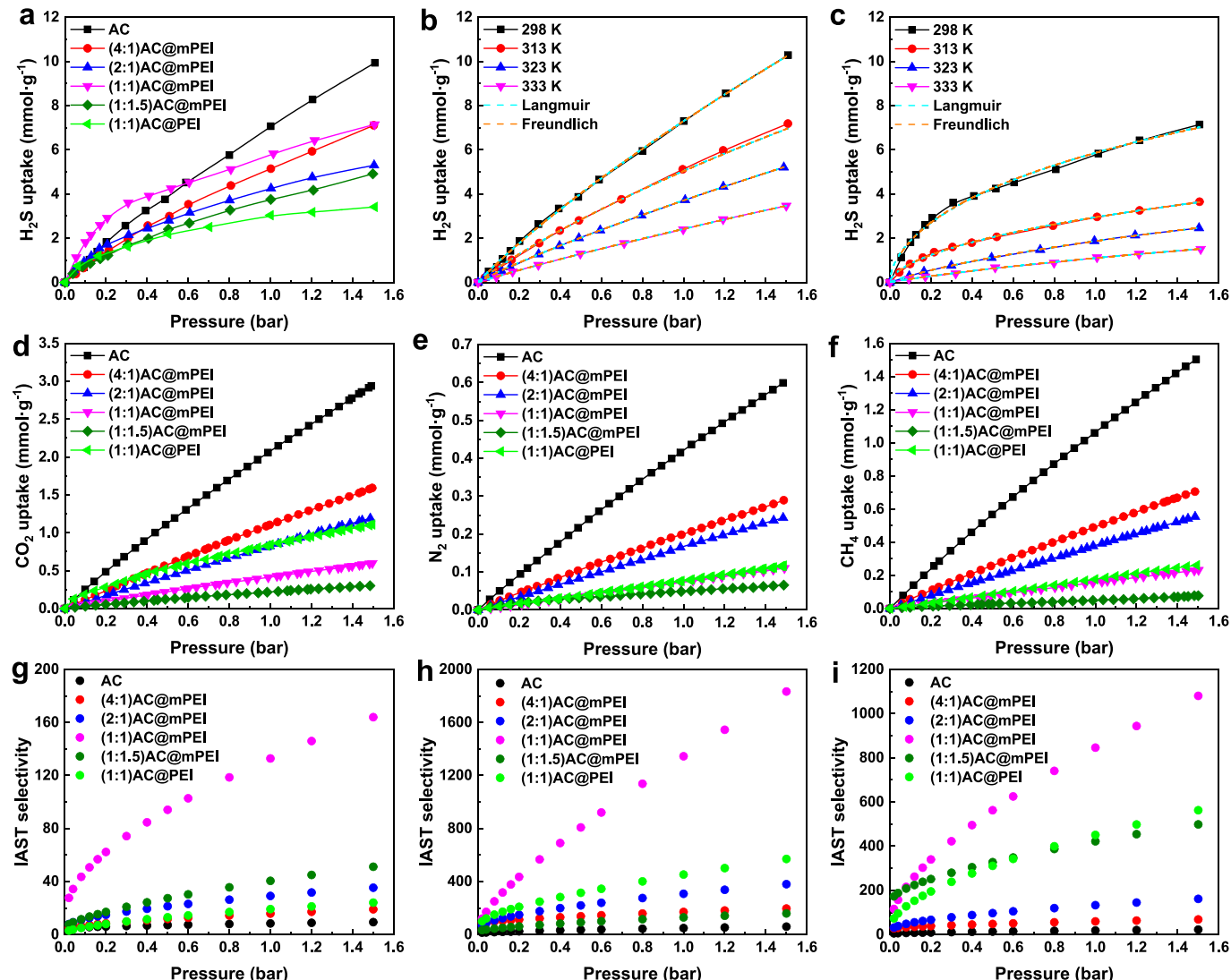


Fig. 5. H₂S adsorption isotherms at 298 K of the adsorbents (a), H₂S adsorption isotherms of AC (b), and (1:1)AC@mPEI (c) at different temperatures, CO₂ adsorption isotherms (d), N₂ adsorption isotherms (e), and CH₄ adsorption isotherms (f) at 298 K of the adsorbents. IAST selectivity of H₂S/CO₂ (2/98) (g), H₂S/N₂ (1/99) (h), and H₂S/CH₄ (10/90) (i) at 298 K of the adsorbents.

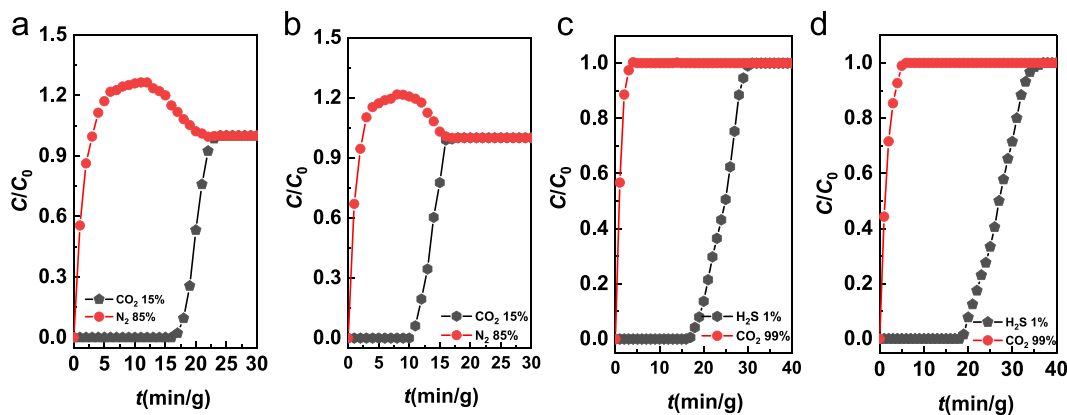


Fig. 6. Breakthrough curves of CO_2/N_2 and $\text{H}_2\text{S}/\text{CO}_2$ mixed gas adsorption on AC (a, c) and (1:1)AC@mPEI (b, d) at 298 K and 1.0 bar.

performance compared to other hybrid adsorbent materials. At extremely low pressures, the H_2S uptake of (1:1)AC@mPEI is significantly higher, indicating that the presence of mPEI on its organization structure provides sufficient interaction between H_2S molecules and the adsorbent. However, there is a significant decrease to $3.76 \text{ mmol}\cdot\text{g}^{-1}$ in the H_2S capacity of (1:1)AC@mPEI, potentially due to the composite adsorbent's solid-liquid mixture viscous state resulting from excessive mPEI addition, which can affect the adsorption process. Overall, these results suggest that introducing an appropriate amount of mPEI is beneficial for H_2S capture. Additionally, (1:1)AC@PEI, serving as a control sample, displays an inferior H_2S adsorption capacity of $3.04 \text{ mmol}\cdot\text{g}^{-1}$ at same conditions.

Fig. 5d exhibits a positive linear correlation between the adsorption isotherms of CO_2 on AC and (x:y)AC@mPEI as a function of pressures. Increasing the mPEI content leads to a gradual decrease in gas adsorption capacities, with (1:1)AC@mPEI exhibiting the lowest CO_2 adsorption. These findings suggest that adding mPEI to AC inhibits the adsorption of CO_2 . This inhibition can be attributed to the weakened interaction between gas molecules and the micro surface of (1:1)AC@mPEI, which is caused by the presence of mPEI and the blockage of numerous micropores in AC. Fig. 5e and f display that the N_2 and CH_4 adsorption curves of (1:1)AC@PEI follow a similar trend as (1:1)AC@mPEI for CO_2 capture. It can be seen from Table 1 that the CO_2 adsorption capacity of (1:1)AC@PEI stands at $0.84 \text{ mmol}\cdot\text{g}^{-1}$ at 1.0 bar, falling short that of AC ($2.15 \text{ mmol}\cdot\text{g}^{-1}$ at 1.0 bar) but surpassing that of (1:1)AC@mPEI ($0.42 \text{ mmol}\cdot\text{g}^{-1}$ at 1.0 bar) under the identical conditions. This discrepancy in adsorption capacity can be attributed to the higher effectiveness of polyamine groups in PEI in attracting CO_2 gas molecules compared to the tertiary amine groups in mPEI.

To further investigate the preferential gas adsorption of prepared adsorbents, the selectivity of $\text{H}_2\text{S}/\text{CO}_2(2/98)$, $\text{H}_2\text{S}/\text{N}_2(1/99)$, and $\text{H}_2\text{S}/\text{CH}_4(10/90)$ at 298 K was calculated according to IAST [48], depicted in Eq.(1):

$$S = \left(\frac{X_1}{Y_1} \right) / \left(\frac{X_2}{Y_2} \right) \quad (1)$$

where S is the IAST selectivity of H_2S over CO_2 , N_2 , or CH_4 ; X is the fraction in the adsorbed phase; Y is the molar fraction in the gas phase.

It can be observed from Fig. 5g-i that the AC shows the lowest selectivity, with IAST selectivity of $\text{H}_2\text{S}/\text{CO}_2(2/98)$, $\text{H}_2\text{S}/\text{N}_2(1/99)$, and $\text{H}_2\text{S}/\text{CH}_4(10/90)$ at 298 K and 1.0 bar being 8, 48, and 18, respectively (Table 1). After incorporating mPEI, the gas selectivity of hybrid adsorbent materials is significantly improved. Remarkably, (1:1)AC@mPEI exhibits the optimal selectivity, with IAST selectivity of $\text{H}_2\text{S}/\text{CO}_2(2/98)$, $\text{H}_2\text{S}/\text{N}_2(1/99)$, and $\text{H}_2\text{S}/\text{CH}_4(10/90)$ at 298 K and 1.0 bar being 133, 1344, and 846, respectively. For (1:1)AC@mPEI, the separation selectivity is enhanced 16.6 times higher than that of the porous carbon supporter. The significant selectivity of H_2S in CO_2 , N_2 , or CH_4

Table 2

The adsorption performance of different carbon-based adsorbents for H_2S at 298 K and 1.0 bar.

Adsorbent	H_2S ($\text{mmol}\cdot\text{g}^{-1}$)	CO_2 ($\text{mmol}\cdot\text{g}^{-1}$)	Selectivity ^a	Ref.
GP123_CO ₂ activ_3h_900C	25.7	6.02	68.2 min ($\text{H}_2\text{S}/\text{CO}_2$) ^b	[32]
JW-NC	17.19	8.05	–	[48]
DP-CN-1-4	13.8	8.3	60 $\text{H}_2\text{S}/\text{N}_2(1/99)$ 65 $\text{H}_2\text{S}/\text{CH}_4(10/90)$	[34]
IANC	12.65	7.23	22.74 ($\text{H}_2\text{S}/\text{CH}_4$)	[49]
KHC-1	205.06 ^c	–	330 min ($\text{H}_2\text{S}/\text{CO}_2$) ^b	[50]
PPy-KOH-700	19.7 ^d	–	4.7 $\text{H}_2\text{S}/\text{CO}_2(0.1:0.1)$	[33]
NPC-1	426.2 ^c	–	–	[51]
CAC450-800	164.54 ^c	–	–	[52]
(1:1)AC@mPEI	5.83	0.43	133 $\text{H}_2\text{S}/\text{CO}_2(2/98)$ 1344 $\text{H}_2\text{S}/\text{N}_2(1/99)$ 846 $\text{H}_2\text{S}/\text{CH}_4(10/90)$	This work

^a IAST selectivity. ^bBreakthrough time. ^cUnit: mg/g. ^d H_2S adsorption capacity was tested at 273 K.

make (1:1)AC@mPEI hybrid adsorbent to be a promising candidate for H_2S removal.

Fig. 6 displays the breakthrough curves of $\text{CO}_2/\text{N}_2(15/85)$ and $\text{H}_2\text{S}/\text{CO}_2(1/99)$ mixed gas adsorption on AC and (1:1)AC@mPEI at 298 K and 1.0 bar. For selective adsorption CO_2 and N_2 , the breakthrough time of CO_2 on AC is about 22 min (Fig. 6a). In contrast, the breakthrough time of (1:1)AC@mPEI significantly shortened to 16 min (Fig. 6b). This implies that the CO_2 adsorption capacity on (1:1)AC@mPEI is inhibited after mPEI modification, potentially due to the pores of adsorbent being filled by mPEI. For selective adsorption H_2S and CO_2 , AC shows a breakthrough time difference of 23 min for $\text{H}_2\text{S}/\text{CO}_2(1/99)$ (Fig. 6c), while (1:1)AC@mPEI displays a breakthrough time difference of 32 min (Fig. 6d). The selective adsorption of H_2S by the hybrid adsorbent was significantly improved, suggesting that adding mPEI contributes to the efficient adsorption of H_2S .

Table 2 shows comparison between the gas selectivity of (1:1)AC@mPEI and those of carbon materials reported in the literature, demonstrating the superior gas selectivity of (1:1)AC@mPEI. Based on previous literature [38,53], the superiority of (1:1)AC@mPEI for selective gas adsorption can be explained as following reasons: (1) the presence of tertiary amine groups in mPEI enhances the interaction of adsorbent and H_2S gas molecules and hinders CO_2 adsorption; and (2)

Table 3Thermodynamic parameters for H₂S adsorption on AC and (1:1)AC@mPEI.

Samples	ΔH^θ (kJ·mol ⁻¹)	ΔS^θ (kJ·mol ⁻¹ ·K)	ΔG^θ (kJ·mol ⁻¹)			
			298 K	313 K	323 K	333 K
AC	-25.51	-0.069	-4.925	-4.259	-3.519	-2.446
(1:1)AC@mPEI	-38.97	-0.116	-4.381	-2.813	-1.679	-0.226

mPEI is immobilized into porous carbon to obtain a composite adsorbent that can overcome the high viscosity of pure mPEI. The abundance of micropores and mesoporous structures in AC provides a specific surface area for loading mPEI.

3.2.3. Adsorption thermodynamics

The adsorption capacity of H₂S on AC and (1:1)AC@mPEI at different temperatures was investigated, respectively. The results shown in Fig. 5b indicate that the H₂S uptake onto AC decreases with increasing temperature. The adsorption curves exhibit a linear relationship with pressure, indicating that the physical adsorption of H₂S is exothermic. Fig. 5c indicates that the H₂S adsorption capacity of (1:1)AC@mPEI significantly increases in the low-pressure region. This can be attributed to chemical interactions dominating at low-pressure, while physical interactions prevail at high-pressure [54]. To further investigate the interaction between H₂S gas molecules and adsorbents, the thermodynamic parameters in adsorption process were collected by fitting the Langmuir (Eq. 2) and Freundlich (Eq. 3) models to adsorption isotherms. The Langmuir and Freundlich parameters for H₂S adsorption on AC and (1:1)AC@mPEI adsorbents are listed in Table S1. Additionally, the isothermal heat of adsorption (ΔH) was also estimated using the Clausius-Clapeyron Eq.(4).

$$q = \frac{q_L k_L p}{1 + k_L p} \quad (2)$$

$$q = k_F(p)^{\frac{1}{n_F}} \quad (3)$$

where q represents the adsorption capacity (mmol·g⁻¹), p is pressure (bar), q_L and k_F are saturated adsorption capacities (mmol·g⁻¹), k_L and n_F are constants of model isotherms (bar⁻¹).

$$\ln(p) = -\frac{\Delta H}{RT} + C \quad (4)$$

where p is pressure (bar), ΔH is the isothermal heat of adsorption (kJ·mol⁻¹), T is temperature (K), R and C are the universal gas constant and the integration constant, respectively.

The ΔH curves of adsorption of H₂S on two adsorbents are shown in Fig. S6. It can be observed that the ΔH of adsorption of H₂S on (1:1)AC@mPEI is higher than that of AC, indicating a stronger interaction between H₂S and (1:1)AC@mPEI. On the other hand, the ΔH of H₂S adsorption on AC shows a decreasing trend as the H₂S uptake increases. This can be attributed to the presence of dispersed strong adsorption active sites on the surface of AC, which dominate the gas-solid interaction. In contrast, the ΔH values increase as the H₂S adsorption increases on (1:1)AC@mPEI. This suggests that the adsorption sites on the adsorbent's surface are rapidly occupied by H₂S molecules, leading to gas-gas interaction dominate and the absence of strong adsorption sites. As the adsorption continues, the ΔH values increase [55]. In short, the loading of mPEI onto the AC to form (1:1)AC@mPEI enhances the presence of strong adsorption sites for H₂S gas molecules, resulting in an enhanced interaction between adsorbate and adsorbent.

The enthalpy change of H₂S adsorption (ΔH^θ) was calculated using the Van't Hoff Eq.(5). The standard Gibbs free energy change (ΔG^θ) and the entropy change (ΔS^θ) were calculated from Eq.s (6) and (7), respectively.

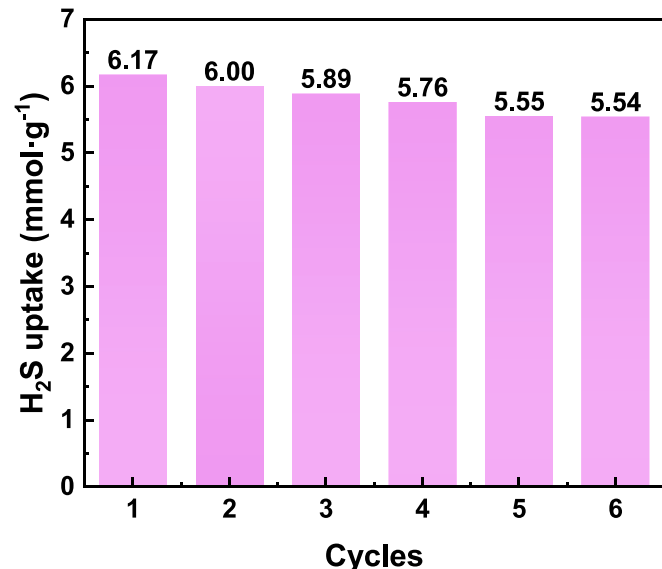


Fig. 7. The recycle performance of (1:1)AC@mPEI for H₂S adsorption at 298 K and 1.2 bar.

$$\frac{\partial \ln(k_F)}{\partial T} = \frac{\Delta H^\theta}{RT^2} \quad (5)$$

$$\ln(k_F) = -\frac{\Delta G^\theta}{RT} \quad (6)$$

$$T\Delta S^\theta = \Delta H^\theta - \Delta G^\theta \quad (7)$$

Table 3 shows that both AC and (1:1)AC@mPEI exhibit negative ΔH^θ values, indicating exothermic H₂S adsorption. The absolute value of ΔH^θ for (1:1)AC@mPEI (-38.97 kJ·mol⁻¹) is much larger than that of AC (-25.51 kJ·mol⁻¹), suggesting a stronger interaction between (1:1)AC@mPEI and H₂S. It should be noted that the ΔH^θ are above 20 kJ·mol⁻¹, but they do not meet the well-defined region of $\Delta H^\theta \geq 40$ kJ·mol⁻¹ for chemisorption [56]. Therefore, this deduction confirms the presence of both physisorption and chemisorption of H₂S on AC and (1:1)AC@mPEI. Additionally, the negative values of ΔS^θ suggest that the adsorption process is orderly. The absolute value of ΔS^θ for AC increases from 0.069 kJ·mol⁻¹·K to 0.116 kJ·mol⁻¹·K for (1:1)AC@mPEI, indicating that the H₂S gas molecules tend to concentrate at the surface of (1:1)AC@mPEI adsorbent. Furthermore, the negative ΔG^θ values indicate thermodynamically favorable and spontaneous H₂S adsorption. These results imply the coexistence of physical and chemical processes in the adsorption of H₂S molecules on both AC and (1:1)AC@mPEI adsorbents.

To assess the cyclic stability of (1:1)AC@mPEI adsorption, a series of continuous H₂S adsorption-desorption experiments were performed. After the adsorption of H₂S on (1:1)AC@mPEI reaches equilibrium at 298 K and 1.2 bar, the desorption of H₂S was degassing at vacuum and 353 K for 180 min until complete removal of the adsorbed H₂S. The recycling performance of (1:1)AC@mPEI for H₂S adsorption at 298 K and 1.2 bar is shown in Fig. 7. After six recycles, the adsorption capacity decreases by about 10 %. This reduction can be attributed to the

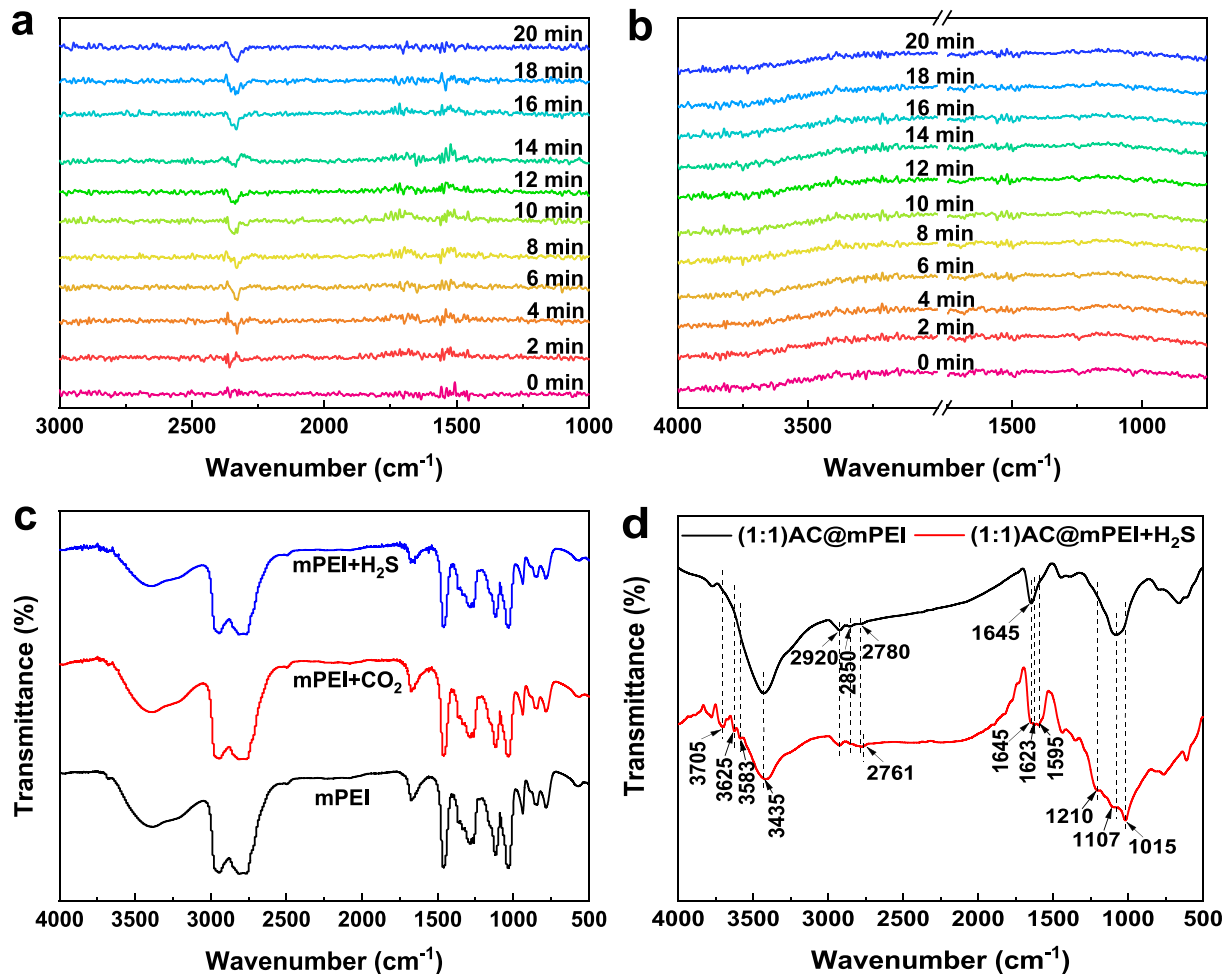


Fig. 8. In-situ FTIR spectra of the (1:1)AC@mPEI recorded under 10 % CO₂ (a) and 4 % H₂S (b) (N₂ as a diluent gas). FTIR spectra of mPEI before and after CO₂ and H₂S capture (c). FTIR spectra of (1:1)AC@mPEI before and after H₂S capture (d).

presence of blocked pores and incompletely regenerated adsorption sites. Even so, the adsorption capacity of H₂S still exceed 5.50 mmol·g⁻¹, surpassing that of most adsorbents reported in the literature.

3.3. Adsorption mechanism

To gain insight into the adsorption mechanism of CO₂ and H₂S on (1:1)AC@mPEI, in-situ FTIR tests were conducted, as shown in Fig. 8a and b. At the same time, individual mPEI was also directly used for the absorption of CO₂ and H₂S to further clarify the promotion mechanism of amines, as shown in Fig. 8c.

Fig. 8a shows that over the course of 20 min, the in-situ FTIR spectra of CO₂ adsorption on (1:1)AC@mPEI demonstrate a gradually increase in the intensity of a main peak at 2335 cm⁻¹, indicative of the asymmetric stretching mode resulting from the physisorption of CO₂ [57,58]. However, the other peaks, particularly in the C-N functional group region, remained unchanged, possibly due to the absence of electron adsorption effect on CO₂ by the tertiary nitrogen functional group. Additionally, Fig. 8c shows no change in the main peak after CO₂ capture by mPEI, suggesting that the tertiary amine groups do not serve as adsorption sites for CO₂ molecules. Overall, the results indicate that the structure property of AC in (1:1)AC@mPEI are crucial in the physicochemical adsorption on CO₂.

Both Fig. 8b and Fig. 8c demonstrate no change in the spectra of H₂S adsorption on (1:1)AC@mPEI. These results are attributed to weak infrared absorption peak of S-H characteristic functional groups [59], which are overshadowed by the strong structural characteristic peaks of

AC and mPEI. Contrarily, Fig. 8d indicates a significant change in the FTIR spectra of (1:1)AC@mPEI + H₂S when (1:1)AC@mPEI is used as the adsorbent. Specifically, the 2920, 2850 and 2780 cm⁻¹ bands of the adsorbent shifted after adsorption of H₂S, with the 2780 cm⁻¹ peak widening, weakening, and shifting to 2761 cm⁻¹. These changes suggest the influence of sulfur on the carbon structure of the adsorbent, indicating the occurrence of adsorption [60]. Moreover, enhanced absorption peaks at 3705, 3625, and 3583 cm⁻¹ indicate adsorption of H₂S at the alkaline sites of (1:1)AC@mPEI [61]. Shen *et al.* [62] conducted a study on the effect of oxygen-containing functional groups of activated carbon on H₂S adsorption using DFT (density functional theory) quantum chemistry method. The results revealed that the oxygen-containing functional groups, such as pyrone, carbonyl, ester, and carboxyl, can serve as the active sites for H₂S adsorption, while the hydroxyl group is not related to the removal of H₂S. Hence, in the presence of these oxygen groups, H₂S can interact with the C=O oxygen atom, leading to the formation of C-S and C-SH species. As expected, the hydroxyl group at 3435 cm⁻¹ did not exhibit significant change in the FTIR spectra, indicated its non-participation in the adsorption mechanism. Conversely, the carbonyl group (C=O) served as an active site for H₂S adsorption. After adsorption of H₂S, the characteristic peak of 1645 cm⁻¹ became noticeably broader and new characteristic peaks at 1623 and 1595 cm⁻¹ appeared in the spectra of (1:1)AC@mPEI + H₂S, potentially linked to the interaction between C=O from AC and H₂S. Additionally, the enhancement of characteristic peaks at 1210 and 1107 cm⁻¹ may be attributed to the electrostatic effect of mPEI's tertiary amine groups on H₂S molecules, while the characteristic peak at 1015 cm⁻¹ may be

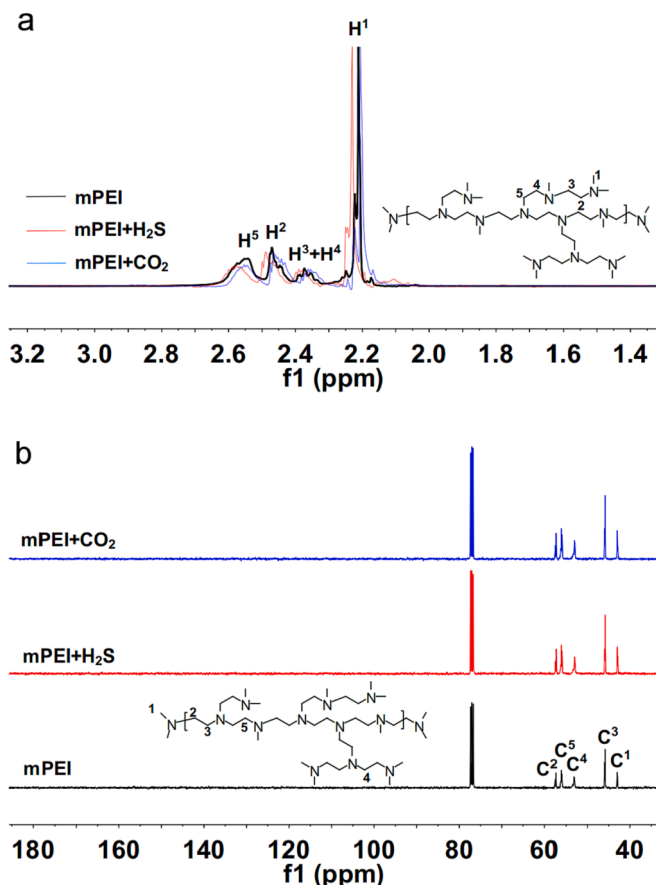


Fig. 9. The ^1H NMR (a) and ^{13}C NMR (b) spectra of mPEI before and after CO_2 and H_2S capture.

related to S-H vibration [63].

Overall, the heteroatoms (including O, N, H) of AC and functional groups of mPEI in the hybrid adsorbent significantly influence the chemical properties of the adsorbent surface, favoring H_2S adsorption. Notably, FTIR characterization results indicated that tertiary amine had a stronger electron adsorption effect on H_2S than on CO_2 . Therefore, mPEI has the potential to enhance H_2S capture in the hybrid adsorbent.

To further investigate the adsorption mechanism of H_2S and CO_2 in mPEI, we conducted a study on the ^1H NMR and ^{13}C NMR spectra for mPEI before and after CO_2 and H_2S capture. Fig. 9a shows that all chemical shifts of the protons on mPEI hardly move after the adsorption of CO_2 . It is noteworthy that the chemical shifts of H^1 , H^2 , and H^5 protons move from 2.20, 2.46, and 2.54 ppm to 2.23, 2.48, and 2.58 ppm after adsorption H_2S , respectively. This phenomenon can be attributed to the dissociation of H_2S into protons H^+ and anion HS^- in the adsorption process, resulting in interaction with tertiary N to form the $[\text{R}_1\text{R}_2\text{R}_3\text{NH}]^+[\text{HS}]^-$ salt, leading to a significant reduction in electron density around the H^1 , H^2 , and H^5 atoms [64].

In Fig. 9b, no pronounced changes were found in ^{13}C NMR before and after adsorption CO_2 and H_2S . Furthermore, there was no chemical shift observed at around 160 ppm in mPEI after the adsorption of CO_2 . A possible explanation for this phenomenon is that the tertiary amine groups does not interact with CO_2 . Based on the results of FTIR and NMR, it is evident that H_2S has a stronger interaction with the tertiary nitrogen atom in mPEI compared to CO_2 , thereby enhancing the separation selectivity between CO_2 and H_2S .

4. Conclusions

In summary, a series of hybrid adsorbent materials, namely (x:y)

AC@mPEI, were designed for the selective adsorption of H_2S from CO_2 , N_2 , and CH_4 gases. These materials exhibited recyclable and excellent H_2S separation properties, with (1:1)AC@mPEI having H_2S adsorption capacity of 5.83 $\text{mmol}\cdot\text{g}^{-1}$ at 298 K and 1.0 bar and ideal selectivity of 133, 1344, and 846 for $\text{H}_2\text{S}/\text{CO}_2$ (2/98), $\text{H}_2\text{S}/\text{N}_2$ (1/98), and $\text{H}_2\text{S}/\text{CH}_4$ (10/90), respectively. The adsorption enthalpy (ΔH^θ) of $-38.97 \text{ kJ}\cdot\text{mol}^{-1}$ implied that the adsorption of H_2S on the (1:1)AC@mPEI involves both physical and chemical processes. This physicochemical interaction between (1:1)AC@mPEI and H_2S was further confirmed through FTIR and NMR. Overall, this novel strategy for H_2S capture establishes a foundation for high-efficiency desulfurization process.

CRediT authorship contribution statement

Lan Luo: Writing – original draft, Investigation. **Chunliang Yang:** Investigation. **Fei Liu:** Visualization, Supervision, Funding acquisition, Conceptualization. **Quanlan Liao:** Investigation. **Peng Chen:** Visualization. **Tianxiang Zhao:** Writing – review & editing, Investigation, Conceptualization.

Declaration of competing interest

The authors declare that they have no known competing financial interests or personal relationships that could have appeared to influence the work reported in this paper.

Data availability

Data will be made available on request.

Acknowledgment

This work was supported by the National Natural Science Foundation of China (nos.22168012 and 22208070), Key Laboratory of Carbon-based Energy Molecular Chemical Utilization Technology in Guizhou Province (no.2023008), Guizhou Provincial Science and Technology Projects (no. ZKZD2023004), Innovation Group Project of Education Department in Guizhou Province (no. 2021010), and the Guizhou Province Outstanding Young Scientific and Technological Talents Program (no.YQK2023007). We also would like to thank the researchers in the Shiyanjia Lab (www.shiyanjia.com) for their helping with SEM and TEM analysis.

Appendix A. Supplementary material

Supplementary data to this article can be found online at <https://doi.org/10.1016/j.seppur.2024.126974>.

References

- [1] M. Pardakhti, T. Jafari, Z. Tobin, B. Dutta, E. Moharreri, N.S. Shemshaki, S. Suib, R. Srivastava, Trends in solid adsorbent materials development for CO_2 capture, *ACS Appl. Mater. Interfaces* 11 (2019) 34533–34559.
- [2] A. Farhadian, W.J. Go, S. Yun, A. Rahimi, M.R. Nabid, D. Iravani, Y. Seo, Efficient dual-function inhibitors for prevention of gas hydrate formation and $\text{CO}_2/\text{H}_2\text{S}$ corrosion inside oil and gas pipelines, *Chem. Engin. J.* 431 (2022) 134098–134112.
- [3] X.W. Ma, L.J. Yang, H. Wu, Removal of volatile organic compounds from the coal-fired flue gas by adsorption on activated carbon, *J. Clean. Prod.* 302 (2021) 126925–126933.
- [4] T.M. Gür, Carbon dioxide emissions, capture, storage and utilization: review of materials, processes and technologies, *Prog. Energy Combust. Sci.* 89 (2022) 100965–101020.
- [5] S.D. Chamberlain, A.R. Ingraffea, J.P. Sparks, Sourcing methane and carbon dioxide emissions from a small city: influence of natural gas leakage and combustion, *Environ. Pollut.* 218 (2016) 102–110.
- [6] Y.C. Chen, Y.B. Wang, Z.F. Yan, J. Deng, G.S. Luo, Selective removal of H_2S over CO_2 in a membrane gas-liquid microdispersion microreactor, *Sep. Purif. Technol.* 314 (2023) 123600–123608.
- [7] Y.H. Chan, S.S.M. Lock, M.K. Wong, C.L. Yiin, A.C.M. Loy, K.W. Cheah, S.Y. W. Chai, C. Li, B.S. How, B.L.F. Chin, S.S. Lam, A state-of-the-art review

- on capture and separation of hazardous hydrogen sulfide (H_2S): recent advances, challenges and outlook, *Environ. Pollut.* 314 (2022) 120219–120238.
- [8] Y. Liu, Z.Y. Liu, B.E. Kraftschik, V.P. Babu, N. Bhuvanai, D. Chinn, W.J. Koros, Natural gas sweetening using TEGMC polyimide hollow fiber membranes, *J. Membr. Sci.* 632 (2021) 119361–119366.
 - [9] Y.L. Wang, X.B. Liu, A. Kraslawski, J. Gao, P.Z. Cui, A novel process design for CO_2 capture and H_2S removal from the syngas using ionic liquid, *J. Clean. Prod.* 213 (2019) 480–490.
 - [10] Y.N. Dong, W.C. Chen, L.L. Zhang, B.C. Sun, G.W. Chu, J.F. Chen, Sulfur recycle in biogas production: novel higee desulfurization process using natural amino acid salts, *Chemosphere* 297 (2022) 134215–134224.
 - [11] D.J. Helderbrant, J. Kothandaraman, N.M. Dowell, L. Brickett, Next steps for solvent-based CO_2 capture; integration of capture, conversion, and mineralisation, *Chem. Sci.* 13 (2022) 6445–6456.
 - [12] X.K. Wu, N.N. Cheng, H.J. Jiang, W.T. Zheng, Y. Chen, K. Huang, F.J. Li, 1-ethyl-3-methylimidazolium chloride plus imidazole deep eutectic solvents as physical solvents for remarkable separation of H_2S from CO_2 , *Sep. Purif. Technol.* 276 (2021) 119313–119321.
 - [13] F.O. Ochedi, J.L. Yu, H. Yu, Y.X. Liu, A. Hussain, Carbon dioxide capture using liquid absorption methods: a review, *Environ. Chem. Lett.* 19 (2021) 77–109.
 - [14] C. Chiappi, C.S. Pomelli, Hydrogen sulfide and ionic liquids: absorption, separation, and oxidation, *Top. Curr. Chem.* 375 (2017) 52–76.
 - [15] X.M. Zhang, W.J. Xiong, M.Z. Shi, Y.T. Wu, X.B. Hu, Task-specific ionic liquids as absorbents and catalysts for efficient capture and conversion of H_2S into value-added mercaptan acids, *Chem. Engin. J.* 408 (2021) 127866–127872.
 - [16] M.A. Rodrigues, J.S. Ribeiro, E.S. Costab, J.L. Mirandab, H.C. Ferraz, Nanostructured membranes containing $UiO-66$ (Zr) and $MIL-101$ (Cr) for O_2/N_2 and CO_2/N_2 separation, *Sep. Purif. Technol.* 192 (2018) 491–500.
 - [17] Z.H. Liu, G. Sun, Z.J. Chen, Y. Ma, K. Qiu, M. Li, B.J. Ni, Anchoring cu-N active sites on functionalized polyacrylonitrile fibers for highly selective H_2S/CO_2 separation, *J. Hazard. Mater.* 450 (2023) 131084–131096.
 - [18] X.Z. Hea, I. Kumakirib, M. Hillestad, Conceptual process design and simulation of membrane systems for integrated natural gas dehydration and sweetening, *Sep. Purif. Technol.* 247 (2020) 116993–117000.
 - [19] M. Liu, M.D. Nothling, S. Zhang, Q. Fu, G.G. Qiao, Thin film composite membranes for postcombustion carbon capture: polymers and beyond, *Prog. Polym. Sci.* 126 (2022) 101504–101543.
 - [20] H.Y. Yang, X.Z. Wang, J. Liu, W.Z. Liu, Y. Gong, Y.K. Sun, Amine-impregnated polymeric resin with high CO_2 adsorption capacity for biogas upgrading, *Chem. Eng. J.* 430 (2022) 132899–132906.
 - [21] H.L. Peng, J.B. Zhang, J.Y. Zhang, F.Y. Zhong, P.K. Wu, K. Huang, J.P. Fan, F.J. Liu, Chitosan-derived mesoporous carbon with ultrahigh pore volume for amine impregnation and highly efficient CO_2 capture, *Chem. Eng. J.* 359 (2019) 1159–1165.
 - [22] J.Y. Zhang, J.B. Zhang, M.J. Li, Z.L. Wu, S. Dai, K. Huang, Solvent-free and one-pot synthesis of ultramicroporous carbons with ultrahigh nitrogen contents for sulfur dioxide capture, *Chem. Eng. J.* 391 (2020) 123579–123587.
 - [23] G. Singh, K.S. Lakhi, S. Sil, S.V. Bhosale, I.Y. Kim, K. Albahily, A. Vinu, Biomass derived porous carbon for CO_2 capture, *Carbon* 148 (2019) 164–186.
 - [24] Q.X. Ma, W.H. Chen, Z.H. Jin, L. Chen, Q.Y. Zhou, X. Jiang, One-step synthesis of microporous nitrogen-doped biochar for efficient removal of CO_2 and H_2S , *Fuel* 289 (2021) 119932–119940.
 - [25] A.E. Ameh, O.O. Oyekola, L.F. Petrik, Column adsorption of rhodamine 6G over NA-P/SOD zeolite synthesised from aluminosilicate secondary waste, *J. Clean. Prod.* 338 (2022) 130571–130580.
 - [26] N. Missaoui, A. Chrouda, H. Kahri, A.J. Gross, M.R. Ardani, A.L. Pang, M. Ahmadipour, PEG-templated synthesis of ultramicroporous n-ZIF-67 nanoparticles with high selectivity for the adsorption and uptake of CO_2 over CH_4 and N_2 , *Sep. Purif. Technol.* 316 (2023) 123755–123767.
 - [27] J. Lee, C.Y. Chuah, W.S. Tan, J. Song, T.H. Bae, 3D-printed monolithic porous adsorbents from a solution-processible, hypercrosslinkable, functionalizable polymer, *Chem. Engin. J.* 427 (2022) 130883–130892.
 - [28] H.M. Gao, Q.Y. Li, S.J. Ren, Progress on CO_2 capture by porous organic polymers, *Curr. Opin. Green Sustain. Chem.* 16 (2019) 33–38.
 - [29] S. Fakhraie, H.R. Rajabi, A. Rashidi, Fabrication and application of novel core-shell $MIL-101(Cr)/UiO-66(Zr)$ nanocrystals for highly selective separation of H_2S and CO_2 , *Chem. Eng. J.* 452 (2023) 139001–139012.
 - [30] H.J. Jun, D.K. Yoo, S.H. Jhung, Metal-organic framework (MOF-808) functionalized with ethyleneamines: selective adsorbent to capture CO_2 under low pressure, *J. CO₂ Util.* 58 (2022) 101932–101940.
 - [31] B.N. Bhadra, S.H. Jhung, Enhancing the oxidative desulfurization efficiency of cobalt-loaded-porous carbon catalyst via nitrogen doping on carbon support, *J. Clean. Prod.* 360 (2022) 132168–132181.
 - [32] S.A. Niclae, P.A. Szilagyi, M.M. Titirici, Soft templating production of porous carbon adsorbents for CO_2 and H_2S capture, *Carbon* 169 (2020) 193–204.
 - [33] X. Liu, G.Q. Zhangsun, Y. Zheng, S.J. Liang, Y.N. Cao, F.J. Liu, Y.H. Xiao, L. L. Jiang, Hierarchical N-doped carbons endowed with structural base sites toward highly selective adsorption and catalytic oxidation of H_2S , *Ind. Eng. Chem. Res.* 60 (2021) 2101–2111.
 - [34] F. Tabarkhoon, H. Abolghasemi, A. Rashidi, M. Bazmi, M.S. Alivand, F. Tabarkhoon, M.V. Farahani, M.D. Esrafil, Synthesis of novel and tunable micro-mesoporous carbon nitrides for ultra-high CO_2 and H_2S capture, *Chem. Eng. J.* 456 (2023) 140973–140983.
 - [35] D.K. Yoo, S.H. Jhung, Selective CO_2 adsorption at low pressure with a zr-based $UiO-67$ metal-organic framework functionalized with aminosilanes, *J. Mater. Chem. A* 10 (2022) 8856–8865.
 - [36] H.C. Lan, J.Y. Zhang, Q.J. Dai, H. Ye, X. Yu Mao, Y.C. Wang, H.L. Peng, J. Du, K. Huang, Highly efficient, selective and reversible capture of sulfur dioxide by methylated-polyethylenimine supported on graphitic carbon nitride, *Chem. Eng. J.* 409 (2021) 127378–127386.
 - [37] H.C. Lan, Y.T. Zou, Y.C. Wang, N.N. Cheng, W.L. Xu, H.L. Peng, K. Huang, L. Y. Kong, J. Du, Meso-macroporous polymer densely functionalized with tertiary amine groups as effective sorbents for SO_2 capture, *Chem. Eng. J.* 422 (2021) 129699–129707.
 - [38] X. Kan, G.Q. Zhang, J. Ma, F.Q. Liu, Y. Tang, F.J. Liu, X.F. Yi, Y.F. Liu, A.M. Zheng, L.L. Jiang, F.S. Xiao, S. Dai, Multiscale co-assembly to meso-macroporous foamed single-crystal metal-organic frameworks for the supported capture of sulfur dioxide, *Adv. Funct. Mater.* 2312044–2312053 (2024).
 - [39] L. Luo, C.L. Yang, F. Liu, T.X. Zhao, Heteroatom-N, S co-doped porous carbons derived from waste biomass as bifunctional materials for enhanced CO_2 adsorption and conversion, *Sep. Purif. Technol.* 320 (2023) 124090–124104.
 - [40] G.H. Zhu, J.M.Y. Carrillo, A. Sujan, C.N. Okonkwo, S. Park, B.G. Sumpter, C. W. Jones, R. Lively, Molecular blends of methylated-poly(ethylenimine) and amorphous porous organic cages for SO_2 adsorption, *J. Mater. Chem. A* 6 (2018) 22043–22052.
 - [41] N. Naga, A. Inagaki, T. Narita, T. Nakano, Quaternary ammonium ionene porous polymers via menschutkin reaction of methylated polyethylenimine and dibromoalkanes, *Mater. Chem. Phys.* 297 (2023) 127409–127417.
 - [42] P. Liu, X.K. Cai, X.M. Zhang, X.M. Wang, M.S. Xu, F. Liu, T.X. Zhao, Rich ether-based protic ionic liquids with low viscosity for selective absorption of SO_2 through multisite interaction, *Ind. Eng. Chem. Res.* 61 (2022) 5971–5983.
 - [43] L.Y. Wang, Y.L. Xu, Z.D. Li, Y.N. Wei, J.P. Wei, CO_2/CH_4 and H_2S/CO_2 selectivity by ionic liquids in natural gas sweetening, *Energy Fuels* 32 (2018) 10–23.
 - [44] J.S. Xu, H. Wang, C. Zhang, X.F. Yang, S.W. Cao, J.G. Yu, M. Shalom, From millimeter to subnanometer: vapo-solid deposition of carbon nitride hierarchical nanostructures directed by supramolecular assembly, *Angew. Chem. Int. Ed.* 56 (2017) 8426–8430.
 - [45] G.M. Peng, L.D. Xing, J. Barrio, M. Volokh, M. Shalom, A general synthesis of porous carbon nitride films with tunable surface area and photophysical properties, *Angew. Chem. Int. Ed.* 57 (2018) 1186–1192.
 - [46] Q. Li, C.S. Chen, C. Li, R.Y. Liu, S. Bi, P.F. Zhang, Y.F. Zhou, Y.Y. Mai, Ordered bicontinuous mesoporous polymeric semiconductor photocatalyst, *ACS Nano* 14 (2020) 13652–13662.
 - [47] J.W. Fu, L. Zhu, X.K. Jiang, K. Liu, Z.H. Wang, X.Q. Qiu, H.M. Li, J.H. Hu, H. Pan, Y.R. Lu, T.S. Chan, M. Liu, Activation of CO_2 on graphitic carbon nitride supported single-atom cobalt sites, *Chem. Eng. J.* 415 (2021) 128982–128989.
 - [48] R. Ahmadi, M.S. Alivand, N.H.M.H. Tehrani, M. Ardjomand, A. Rashidi, M. Rafizadeh, A. Seif, M. Mollakazemi, Z. Noorpoor, J. Rudd, Preparation of fiber-like nanoporous carbon from jute thread waste for superior CO_2 and H_2S removal from natural gas: experimental and DFT study, *Chem. Eng. J.* 415 (2021) 129076–129090.
 - [49] N.H.M.H. Tehrani, M.S. Alivanda, D.M. Maklavyany, A. Rashidi, M. Samipoorgiri, A. Seif, Z. Yousefian, Novel asphaltene-derived nanoporous carbon with N-S-rich micromesoporous structure for superior gas adsorption: experimental and DFT study, *Chem. Eng. J.* 358 (2019) 1126–1138.
 - [50] W.H. Chen, G.C. Zhang, D. Li, S.G. Ma, B.D. Wang, X. Jiang, Preparation of nitrogen-doped porous carbon from waste polyurethane foam by hydrothermal carbonization for H_2S adsorption, *Ind. Eng. Chem. Res.* 59 (2020) 7447–7456.
 - [51] L. Chen, J. Yuan, T.B. Li, X. Jiang, S.G. Ma, W.L. Cen, W.J. Jiang, A regenerable N-rich hierarchical porous carbon synthesized from waste biomass for H_2S removal at room temperature, *Sci. Total Environ.* 768 (2021) 144452–144461.
 - [52] T.B. Gebregziabher, S. Wang, H. Namd, Adsorption of H_2S , NH_3 and TMA from indoor air using porous corn cob activated carbon: isotherm and kinetics study, *J. Environ. Chem. Eng.* 7 (2019) 103234–103244.
 - [53] K. Huang, J.Y. Zhang, X.B. Hu, Y.T. Wu, Absorption of H_2S and CO_2 in aqueous solutions of tertiary-amine functionalized protic ionic liquids, *Energy Fuels* 31 (2017) 14060–14069.
 - [54] P. Liu, X.K. Cai, X.M. Zhang, T.X. Zhao, Effective absorption of SO_2 by imidazole-based protic ionic liquids with multiple active sites: thermodynamic and mechanical studies, *AIChE J.* 68 (2022) 17596–17608.
 - [55] M.B. Kim, T.U. Yoon, D.Y. Hong, S.Y. Kim, S.J. Lee, S.I. Kim, S.K. Lee, J.S. Chang, Y.S. Bae, High SF_6/N_2 selectivity in a hydrothermally stable zirconium-based metal-organic framework, *Chem. Eng. J.* 276 (2015) 315–321.
 - [56] R.I. Yousef, B. El-Eswed, A.H. Al-Muhtaseb, Adsorption characteristics of natural zeolites as solid adsorbents for phenol removal from aqueous solutions: kinetics, mechanism, and thermodynamics studies, *Chem. Eng. J.* 171 (2011) 1143–1149.
 - [57] S. Wang, Y.R. Lee, Y. Won, H. Kim, S.E. Jeong, B.W. Hwang, A.R. Cho, J.Y. Kim, Y. C. Park, H. Nam, D.H. Lee, H. Kim, S.H. Jo, Development of high-performance adsorbent using KOH-impregnated rice husk-based activated carbon for indoor CO_2 adsorption, *Chem. Eng. J.* 437 (2022) 135378–135393.
 - [58] C. Vittoni, G. Gatti, G. Paul, E. Mangano, S. Brandani, C. Bisio, L. Marchese, Non-porous versus mesoporous siliceous materials for CO_2 capture, *Chemistryopen* 8 (2019) 719–727.
 - [59] E. Isoniemi, M. Pettersson, L. Khriachtchev, J. Lundell, M. Rasanan, Infrared spectroscopy of H_2S and SH in rare-gas matrixes, *J. Phys. Chem. A* 103 (1999) 679–685.
 - [60] F.B. Scheufele, E.S. Silva, B.B. Cazula, D.S. Marins, R. Sequinel, C.E. Borba, G. S. Patuzzo, T.F.M. Lopez, H.J. Alves, Mathematical modeling of low-pressure H_2S adsorption by babassu biochar in fixed bed column, *J. Environ. Chem. Eng.* 9 (2021) 105042–105056.

- [61] L.J. Pei, J.X. Cao, F. Liu, A.J. Yang, M.Q. Yao, T.X. Zhao, X.D. Wang, S. Kawi, Thiolation behaviors of methanol catalyzed by bifunctional ZSM-5@ t-ZrO_2 catalyst, *Catal. Today* 397–399 (2022) 379–388.
- [62] F.H. Shen, J. Liu, C.K. Gu, D.W. Wu, Roles of oxygen functional groups in hydrogen sulfide adsorption on activated carbon surface: a density functional study, *Ind. Eng. Chem. Res.* 58 (2019) 5526–5532.
- [63] N.B. Colthup, Spectra-structure correlations in the infra-red region, *J. Opt. Soc. Am.* 40 (1950) 397.
- [64] Z.Y. Xu, W.B. Zhao, X.H. Xie, Y.H. Li, Y. Chen, Phase-change reversible absorption of hydrogen sulfide by the superbase 1,5-diazabicyclo[4.3.0]non-5-ene in organic solvents, *Ind. Eng. Chem. Res.* 58 (2019) 1701–1710.